High-resolution EELS study of carbon and boron allotropes

Masami Terauchi and Michiyoshi Tanaka

Research Institute for Scientific Measurements, Tohoku University, 2-1-1 Katahira Aoba-ku,Sendai 980, Japan

(Received: Feb. 3, 1997 Accepted: Feb. 19, 1997)

Abstract

We have investigated the electronic structure of carbon allotropes (C_{60}, C_{70}, C_{76}, C_{84} and carbon nanotubes) and boron allotropes (α, β-rhombohedral boron and amorphous boron) using a high-resolution electron energy-loss spectroscopy microscope. Dielectric functions of those materials were derived from the loss functions by Kramers-Kronig analysis. The dielectric function of each allotrope showed a characteristic feature in an energy region below 10eV. The near edge structures of 1*s* electron excitation spectra,which gives partial density of states with *p* symmetry of the conduction band,showed characteristic features for the different allotropes.

1. Introduction

Since Kroto *et al.* [1] discovered a new form of carbon, "fullerene", such as C_{60}, great interest was focused on its crystal structure [1, 2] and optical properties [1, 3] and the superconductivity of the alkali-metal-doped C_{60} crystals [4, 5]. After the recent successful isolation and extraction of macroscopic amounts of higher fullerenes, such as C_{70}, C_{76} and C_{84}, many researches have been conducted on the studies of their structures and electronic properties. Iijima [6, 7] discovered graphitic carbon needles, called "carbon nanotubes". It is interesting to reveal the change of the electronic structures of C_n with the change of n and that of nanotubes with the change of the diameter of the tubes. On the other hand, boron forms four allotropes of α-rhombohedral-boron (α-r-B), α-tetragonal-boron, β-rhombohedral-boron (β-r-B) and β-tetragonal-boron [8] , which are constructed by B_{12} icosahedral clusters. Amorphous boron (am-B) is also constructed by B_{12} icosahedral clusters [9, 10]. The crystal structure of α-r-B is the simplest among the boron allotropes but its electronic structure has not been revealed except the band gap energy [11] because the preparation of the single crystals with a millimeter size was difficult [12].

The present paper reports electron energy-loss spectra obtained from carbon allotropes (C_{60}, C_{70}, C_{76}, C_{84} and carbon nanotubes) and boron allotropes (α-r-B, β-r-B and am-B). The dielectric functions of these materials are derived by Kramers-Kronig analysis of the spectra. The results are compared with energy band calculations.

2. Experimental

C_n (n = 60, 70, 76 and 84) powder was produced by the d.c. arc-dischargeeVaporation of carbon and by the liquid chromatography method. Crystalline thin films of the C_n were grown on mica substrates by evaporating the C_n powder in a vacuum chamber. Specimens for electron energy-loss spectroscopy (EELS) were prepared by peeling the film from the substrate in water and by mounting it on a specimen-supporting copper-mesh covered with a microgrid for transmission electron microscopy. Specimens of carbon nanotubes, which were produced by the d.c. arc-discharge evaporation of carbon, were prepared by dropping a droplet of alcohol containing nanotubes onto a specimen-supporting copper-mesh covered with a microgrid.

Single crystalline specimens of α-r-B and β-r-B were produced by annealing am-B powder, which was prepared by electron-beam evaporation of boron. The specimens were composed of small single crystals of α-r-B (20-40μm), β-r-B (50-100μm) and uncrystallized am-B. The small crystals were crushed and put in alcohol. Specimens for EELS experiments were prepared by dropping a droplet of alcohol containing the fragments of boron crystals onto a specimen-supporting copper-mesh covered with a microgrid.

For EELS experiments, specimen areas of the carbon and boron allotropes showing high quality electron diffraction patterns were used. EELS spectra were obtained from specimen areas of 180nm in diameter with a thickness of about 100nm. A high-resolution EELS microscope used was developed as a project of Joint Research with Industry by the Ministry of

Education, Science, Sports and Culture [13, 14]. It is equipped with a thermal-type field emission gun as the electron source and specially-designed double-focus Wien filters as the monochromator and analyzer. The electron energy-loss spectra were detected by a parallel-recording system with a charge-coupled device (CCD) camera. The best values of the full widths at half maximum (FWHM) of the zero-loss peak at present are 15meV and 25meV for the cases without and with a specimen, respectively. The accelerating voltage of incident electrons at the specimen was set at 60keV.

3. Carbon allotropes

3. 1 C_{60}, C_{70}, C_{76} and C_{84} [15, 16, 17, 18]

Figure 1 shows EELS spectra of C_n (n = 60, 70, 76 and 84) together with that of graphite in an energy region of 0–40eV. The energy resolutions were 0.15–0.35eV for the FWHM of the zero-loss peaks. The prominent peaks at 6.5eV for C_{60}, 6.4eV for C_{70}, 6.2eV for C_{76}, 6.1eV for C_{84} and 7.0eV for graphite are interband plasmons (π plasmons) caused by the interband transition of $\pi \rightarrow \pi^*$. The energies of the peaks of C_n are a little lower than that of graphite. Few peaks and/or shoulders are seen on the shoulders of the π plasmon peaks of C_{60}, C_{70}, C_{76} and C_{84}. These structures are also attributed to interband transitions of $\pi \rightarrow \pi^*$. The shoulders in the spectra of C_n (n = 70, 76 and 84) are broader than that of C_{60}. The broadening originates from the removal of the degeneracy of energy levels owing to the lower symmetry of the C_n (n = 70, 76 and 84) clusters than that of the C_{60} cluster. The prominent peaks at 25.5eV for C_{60}, 24.5eV for C_{70}, 24.9eV for C_{76}, 25.5eV for C_{84} and 27.0eV for graphite correspond to volume plasmons ($\pi + \sigma$ plasmons) caused by the collective excitation of whole valence electrons. The peak energies are a little lower than that of graphite. The energies are slightly different from each other. The energies of the $\pi + \sigma$ plasmon peaks for C_{60}, C_{70}, C_{76} and C_{84} calculated by the Lorentz model using the $\pi \rightarrow \pi^*$ and $\sigma \rightarrow \sigma^*$ interband transition energies determined from the imaginary part ε_2 of the dielectric functions of C_n show good agreement with the experimental values.

Figure 2 shows ε_2 of C_n (n = 60, 70, 76 and 84) obtained by Kramers-Kronig analysis of the loss functions in an energy region of 0–8eV. The loss functions were obtained by removing the contributions of multiple scattering using the Fourier-Log deconvolution method [19] . The absolute value of the loss function for each

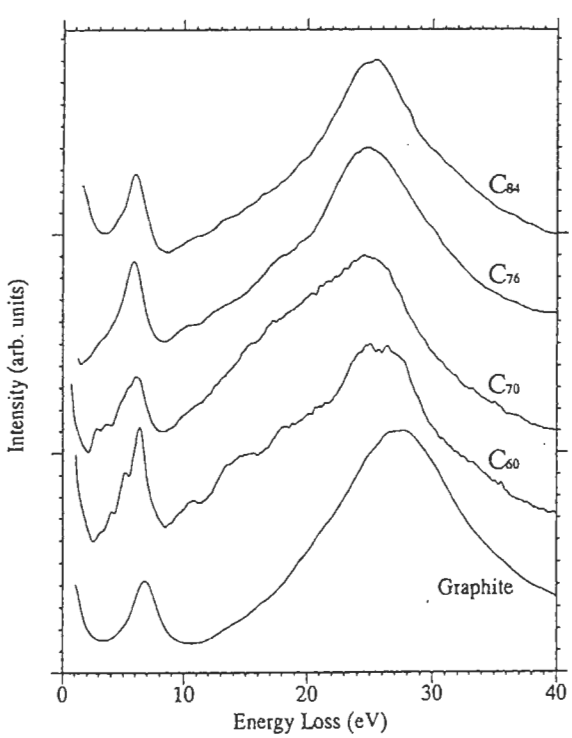

Fig. 1 Electron energy-loss spectra of C_n (n = 60, 70, 76 and 84) together with that of graphite in an energy region of 0–40eV. The energy resolutions were 0.15–0.35eV for the FWHM of the zero-loss peaks.

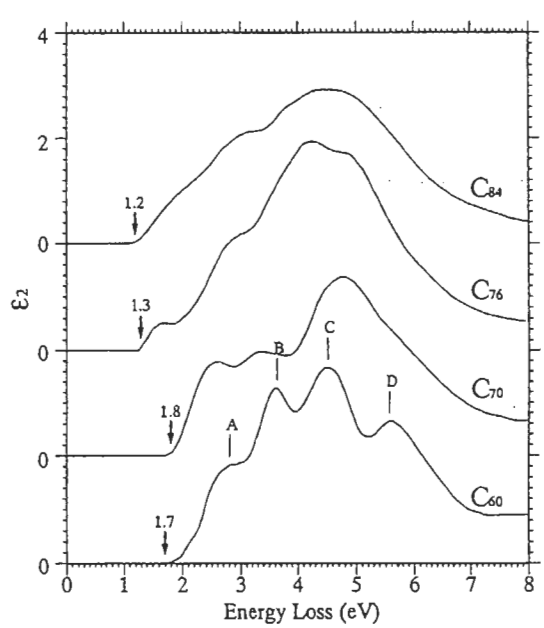

Fig. 2 Imaginary part (ε_2) of the dielectric function of C_n (n = 60, 70, 76 and 84) obtained by Kramers-Kronig analysis of the loss functions in an energy region of 0–8eV.

C_n (n = 60, 70 and 84) was determined by the condition $\mathrm{Re}[-1/\varepsilon(0)] \simeq -1/\varepsilon_1(0) = -1/n^2$, where n is the refractive index. Since the refractive index of C_{76} was not known, the absolute value of the loss function was determined by the sum rule [20]. In the course of Kramers-Kronig analysis of the loss function, the integration with respect to energy was carried out up to 400eV, where the loss function in a higher energy region was extrapolated by using an equation AE^{-4}.

The peaks of C_{60} at 2–7eV (indicated by A–D) were assigned to the individual $\pi \rightarrow \pi^*$ interband transitions of A: $h_u \rightarrow t_{1g}$, B: g_g, $h_g \rightarrow t_{1u}$, C: $h_u \rightarrow h_g$ and D: g_g, $h_g \rightarrow t_{2u}$ by comparing with the band calculation due to Saito and Oshiyama [21]. The peaks in the fullerenes other than C_{60} are broadened by the removal of the degeneracy of the π electron-energy states due to lower symmetries of the C_n clusters than that of the C_{60} cluster. The onset energies at about 1.7eV for C_{60} , 1.8eV for C_{70}, 1.2eV for C_{76} and 1.2eV for C_{84} indicated by arrows are assigned each to the single-electron excitation energy from the highest occupied molecular orbital (HOMO) to the lowest unoccupied molecular orbital (LUMO) (band gap energy). The value of C_{60}, 1.7eV, is very close to a calculated band gap energy of 1.5eV [21]. The smaller band gap energies of C_{76} and C_{84} than those of C_{60} and C_{70} are understood by the removal of the degeneracy of HOMO and LUMO due to lower symmetries of the C_{76} and C_{84} clusters than that of the C_{60} and C_{70} clusters.

Figure 3 shows carbon K-shell excitation spectra (C K-edge) of C_n (n = 60, 70, 76 and 84) together with that of graphite in an energy region of 283–296eV measured with an energy resolution of 0.23eV for the FWHM of the zero-loss peak. Since the carbon 1s core level can be assumed to be flat, these fine structures in the spectra display the density of states of the conduction band. The fine structures observed between 284eV and 290eV and those observed above 290eV are attributed to the transitions from the carbon 1s core level to the unoccupied π^* and σ^* levels, respectively.

The spectral peaks in an energy region of 284–290eV become broad and unseparated on going from C_{60} and C_{70} to C_{76} and C_{84}. This fact is again explained by the removal of the degeneracy of the unoccupied π^* levels due to the lower symmetry of C_{76} and C_{84} clusters. The spectral peaks in an energy region above

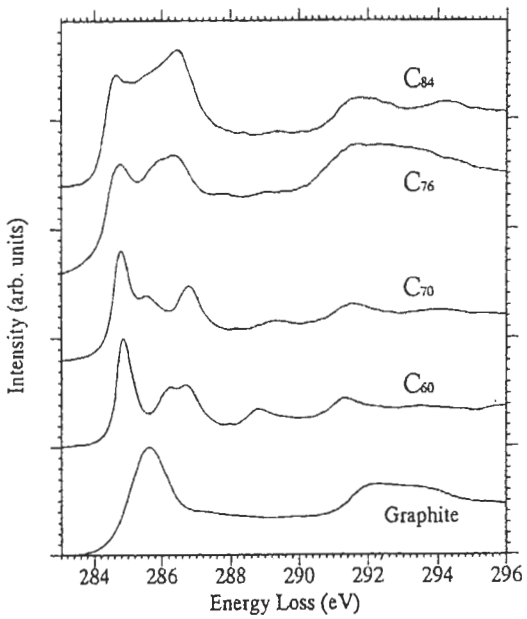

Fig. 3 Carbon K-edge spectra of C_n (n = 60, 70, 76 and 84) together with that of graphite in an energy region of 283–296eV measured with an energy resolution of 0.23eV for the FWHM of the zero-loss peak. The fine structures observed between 284eV and 290eV and those observed above 290eV are attributed to the transitions from the carbon 1s core level to the unoccupied π^* and σ^* levels, respectively.

290eV show no significant difference among C_n (n = 60, 70, 76 and 84). This suggests that the σ^* electron energy levels are not so much affected by the lowering of symmetry of fullerene clusters.

3.2 Single- and multi-shell carbon nanotubes [22, 16, 23]

Figure 4 shows EELS spectra of a bundle of single-shell carbon nanotubes of 1nm diameter (SS-tubes) and a multi-shell carbon nanotube (MS-tube) of 31nm diameter and that of graphite in an energy region of 0–45eV. The energy resolution was 0.27eV. The peaks at 5.8eV for SS-tubes, 6.4eV for an MS-tube and 7.0eV for graphite are interband plasmons (π plasmons) caused by the interband transition of $\pi \rightarrow \pi^*$. MS-tubes with diameters larger than about 20nm showed a π plasmon energy of about 6.4eV. Those having smaller diameters than about 20nm showed a π plasmon peak at about 5.2eV. The larger peaks at 20.6eV for SS-tubes, 22.6eV for an MS-tube and 27.0eV for graphite correspond to volume plasmons ($\pi + \sigma$ plasmons) due to the collective excitation of whole valence electrons. It was found from

electron diffraction experiments that SS-tubes form a hexagonal packing. The low $\pi + \sigma$ plasmon energy of the bundle of SS-tubes is explained by the density of valence electrons calculated on the basis of the hexagonal packing of SS-tubes. The plasmon energy of the MS-tubes is explained by averaging those of graphite obtained at the electron incidences parallel (27eV) and perpendicular (20eV) to the c-axis.

Figure 5 shows C K-edges of a bundle of SS-tubes, an MS-tube and graphite in an energy range of 280–299eV. The energy resolution was 0.4eV. The peaks observed at about 285.5eV are attributed to the transitions from the carbon 1*s* core level to the unoccupied π^* levels. The transition peak of the MS-tube is slightly broader than that of graphite. Since the carbon 1*s* core level can be assumed to be flat, the broadening of the peak indicates the broadening of π^* levels, which is caused by the removal of the degeneracy of π^* levels due to the curving of the graphitic sheets. The peak of the SS-tubes is much broader than that of the MS-tube. The broader peak of the SS-tubes may be attributed to the stronger curving of the graphitic sheet. Stéphan *et al.*, however, obtained C K-edge spectra of an MS-tube and a single SS-tube with an energy resolution of about 0.7eV, and found the broadening of the π^* transition peaks of the tubes are almost the same [24]. The spectrum of the SS-tubes in Fig. 5 was obtained from a bundle of SS-tubes. Thus, the broader feature of the π^* peak of the SS-tubes than that of the MS-tube in Fig. 5 may be due to the interaction among the π^* orbitals of SS-tubes which form the bundle.

4. Boron allotropes [25]

Figure 6 shows EELS spectra of α-r-B, β-r-B and am-B in an energy range of 0–40eV. Energy resolutions of these spectra were 0.18–0.19eV. The steep decrease of spectral intensities around 1eV is the tail of the zero-loss peak. The onset energies of the spectra (band gap energies) of β-r-B and am-B are respectively 1.6eV and 1.4eV, which show good agreement with the values of 1.56eV for β-r-B [26] and 1.32eV for am-B [27] obtained by optical measurements. The onset energy of α-r-B is 2.4eV as indicated by an arrow, which is larger than those of β-r-B and am-B and is also larger by 0.4eV than that of Horn[11] (~2eV) obtained by an optical measurement. Theoretical calculations provided the minimum indirect and

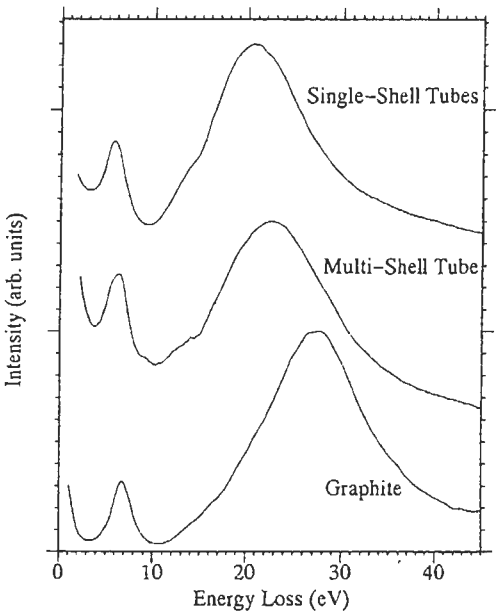

Fig. 4 Electron energy-loss spectra of a bundle of single-shell carbon nanotubes of 1nm diameter (SS-tubes) and a multi-shell carbon nanotube (MS-tube) of 31nm diameter and that of graphite in an energy region of 0–45eV. The energy resolution was 0.27eV.

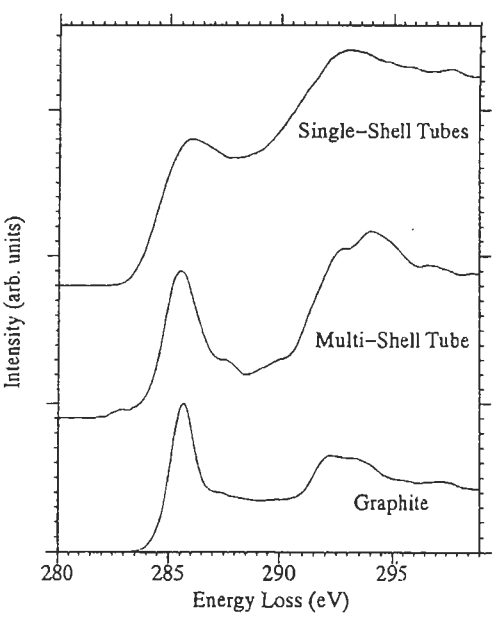

Fig. 5 Carbon K-edge spectra of a bundle of SS-tubes, an MS-tube and graphite in an energy region of 280–299eV. The energy resolution was 0.4eV.

the minimum direct interband transition energies to be about 1.7eV and 2.2–2.3eV, respectively [28, 29, 30]. Since the oscillator strength of the direct interband transition is much larger than that of the indirect transition, the onset observed can be assigned to the minimum direct interband transition energy.

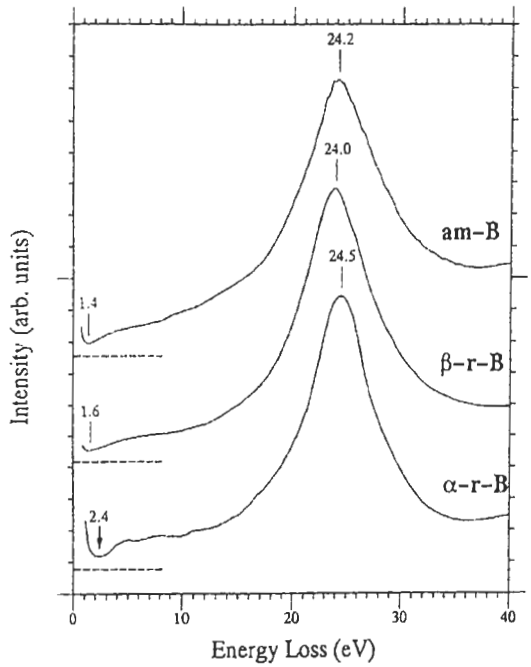

Fig. 6 Electron energy-loss spectrum of α-r-B in an energy range of 1–40eV together with spectra of β-r-B and am-B for comparison. Energy resolutions were 0.18–0.19eV.

The peaks observed at 24.5eV for α-r-B, 24.0eV for β-r-B and 24.2eV for am-B correspond to the volume plasmon caused by the collective excitation of whole valence electrons. These values are close each other because the densities of valence electrons are similar among the three materials.

The spectrum only due to single scattering process was obtained from the experimental spectrum by removing the contribution of the direct beam using a Lorentz fit and that of the multiple scattering part using the Fourier-log deconvolution method. The loss-function was obtained by applying the sum rule to the single scattering spectrum. The dielectric function was derived from the loss-function by Kramers-Kronig analysis. In applying the sum rule to obtain the loss function and in the Kramers-Kronig analysis, the integrations with energy were carried out up to 400eV, where the intensities above 60eV were obtained by extrapolation using an E^{-3} intensity dependence.

Figure 7(a) shows the real part ε_1 and imaginary part ε_2 of the dielectric function of α-r-B, β-r-B and am-B in an energy range of 0–30eV. The condition for the plasmon excitation, $\varepsilon_1 = 0$, is satisfied at 23.3eV for α-r-B, 23.0eV for β-r-B and 22.9eV for am-B. This confirms that the peaks at 24–25eV in Fig. 6 correspond to the volume plasmon excitation. The FWHM values of the volume plasmon peaks of the present boron allotropes (*sp* semiconductors) were 7.5eV for α-r-B, 8.5eV for β-r-B and 10eV for am-B. These values are about twice those of *sp* semiconductors Si and Ge (~4eV). The large FWHM values indicate a strong damping of the volume plasmon due to large values of ε_2 at the energy of $\varepsilon_1 = 0$. The values of $\varepsilon_1(0)$ were 6.5 for α-r-B, 9.3 for β-r-B and 9.4 for am-B. That the value for a-r-B is smaller than the values for β-r-B and am-B is explained by a larger band gap energy of α-r-B than those of β-r-B and

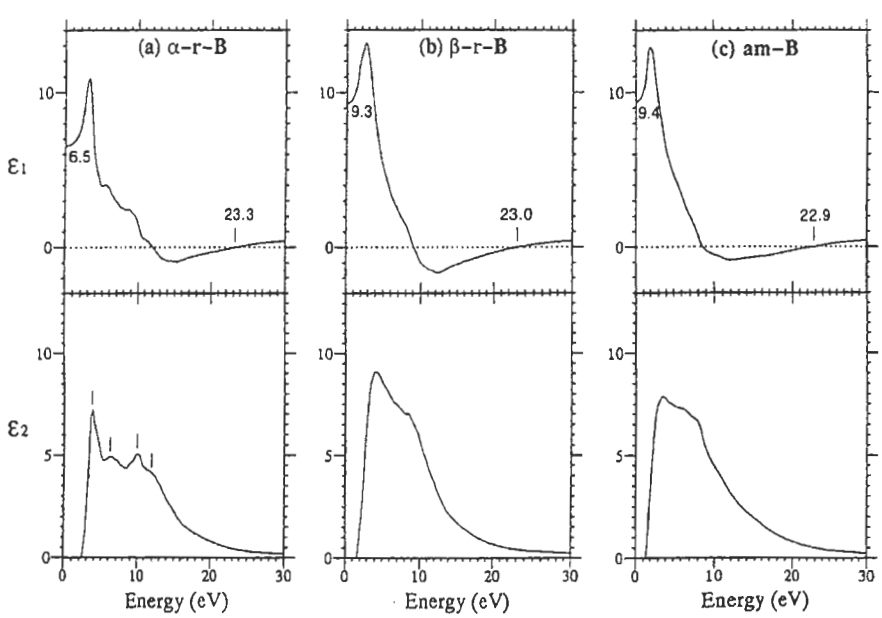

Fig. 7 Real part ε_1 and imaginary part ε_2 of the dielectric function of α-r-B in an energy range of 0–30eV together with those of β-r-B and am-B for comparison.

am-B. ε_2 of α-r-B shows four peaks and/or shoulders (indicated by vertical lines) due to interband transitions, which were not observed in ε_2 of β-r-B and am-B.

Figure 8(a) shows boron K-shell excitation spectra (B K-edge) of α-r-B, β-r-B and am-B in an energy range of 185–205eV. Energy resolutions of the spectra were about 0.2eV. The onsets of the B K-edge were observed at 188.6eV for α-r-B, 187.8eV for β-r-B and 187.4eV for am-B. The larger onset energy of α-r-B than those of β-r-B and am-B should be attributed to the fact that the band gap energy of α-r-B is larger than those of β-r-B and am-B. The B K-edge of α-r-B shows clear peaks, but the spectra of β-r-B and am-B do not. This indicates that there exist clear peaks in the density of states (DOS) of the conduction band of α-r-B. The appearance of the clear peaks in Fig. 8(a) is explained by the fact that all the B_{12} clusters in α-r-B are deformed in the same manner, while the clusters in β-r-B are deformed in four different shapes [31]. The superposition of four different spectra originating from four deformations can smear out the clear peaks in the case of β-r-B. The intensity profile of B K-edge of am-B is similar to that of β-r-B. This indicates that the basic structures of am-B and β-r-B are the same, which is consistent with the analysis of the radial distribution functions of boron allotropes by Kobayashi [10]. Figure 8(b) shows the B K-edge of α-r-B and the density of states of unoccupied states of α-r-B obtained by Gunji [32] using an *ab initio* calculation method under the local density approximation [33]. Gunji assigned peaks A and B to the B2*s*–2*p* hybridized states and the B2*p* state, respectively. The experimental peak positions show good agreement with the peak positions in the calculated density of states. The experimental peak intensity at 189.6eV is much smaller than the intensity in the calculated density of states. Since the B K-edge spectrum was obtained under the condition of dipole transition, the partial density of states with *p* character in unoccupied states was observed. Thus, the experimental peak intensity at 189.6eV is smaller than the intensity in the calculated density of states, which also includes the states with *s*-character.

The present study successfully revealed the

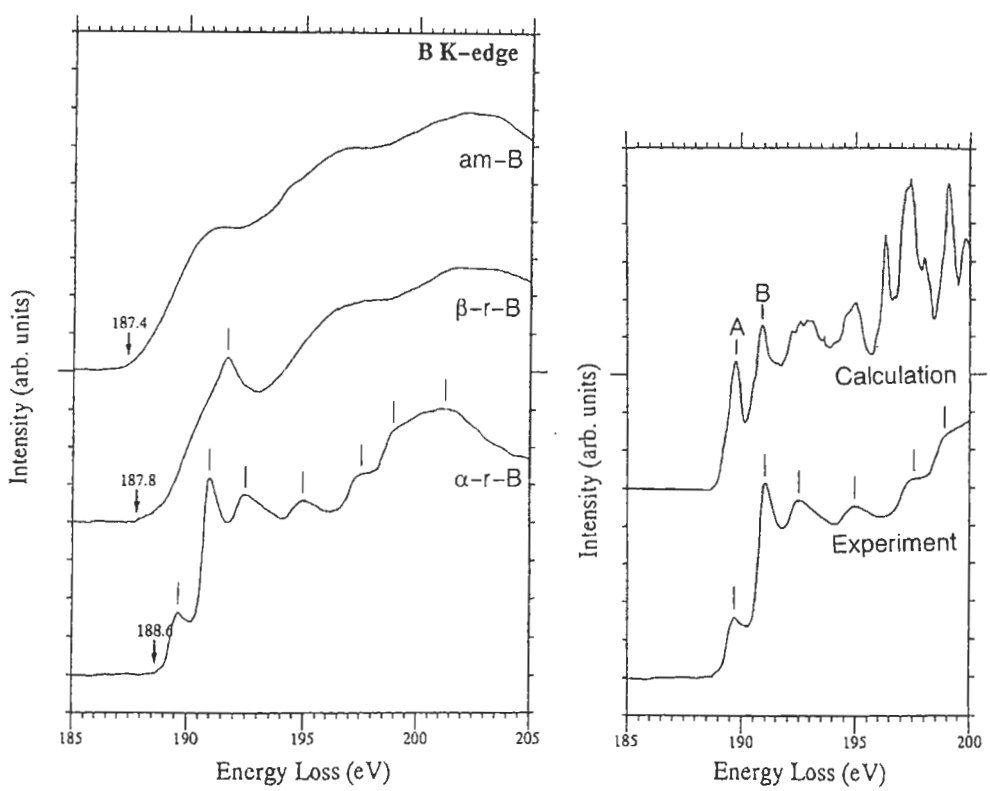

Fig. 8 (a) Boron K-shell excitation spectrum (B K-edge) of α-r-B in an energy range of 185–205eV together with spectra of β-r-B and am-B for comparison. Energy resolutions for the spectra were about 0.2eV.
(b) B K-edge of α-r-B and the density of states of the conduction band of α-r-B obtained by an *ab initio* calculation method under the local density approximation [32, 33] .

difference of the electronic structures of C_n for different n and that of nanotubes for different tube diameters, and the electronic structure of α-r-B by taking the high-resolution electron energy-loss spectra from high-quality single crystalline areas.

Acknowledgements

The authors thank Dr. Y. Saito of Mie Univ. for supplying the C_n single crystals and carbon nanotubes and Dr. K. Kimura of Univ. of Tokyo for supplying the single crystals of boron. Thanks are also due to Dr. Y. Harada, Mr. M. Ishida and Dr. K. Tsuno of JEOL Ltd. for their great effort in constructing the high-resolution EELS microscope. They thank Mr. F. Sato for his skillful technical assistance. The present work was mainly supported by a Grant-in-Aid from the Ministry of Education, Science, Sports and Culture, Japan.

References

1. H. W. Kroto, J. R. Heath, S. C. O'Berin, R. F. Curl and R. E. Smalley, Nature, **318** (1985) 162.
2. R. M. Fleming, T. Siegrist, P. Marsh, B. Hessen, A. R. Kortan, D. W. Murphy, R. C. Haddon, R. Tycko, G. Dabbaghg, A. M. Mujsce, M. L. Kaplan and S. M. Zahurak, Res. Soc. Symp. Proc., **206** (1991) 691.
3. A. F. Hebard, R. C. Haddon, R. M. Fleming and A. R. Kortan, Appl. Phys. Lett., **59** (1991) 2109.
4. A. F. Hebard, M. J. Rosseinsky, R. C. Haddon, D. W. Murphy S. H. Glarum, T. T. M. Palstra, A. P. Ramirez and A. R. Kortan, Nature, **350** (1991) 600.
5. M. J. Rosseinsky, A. P. Ramirez, S. H. Glarum, D. W. Murphy, R. C. Haddon, A. F. Hebard, T. Y. M. Palstra, A. R. Kortan, S. M. Zahurak and A. V. Makhija, Phys. Rev. Lett., **66** (1991) 2839.
6. S. Iijima, Nature, **354** (1991) 56.
7. S. Iijima and T. Ichihashi, Nature, **363** (1993) 603.
8. O. A. Golicova, Phys. stat. sol., **101** (1987) 277.
9. K. Katada, Jpn. J. Appl. Phys., **5** (1966) 582.
10. M. Kobayashi, J. Mat. Sci., **23** (1988) 4392.
11. F. H. Horn, J. Appl. Phys. **30**, 1611 (1959).
12. H. Werheitet, U. Kuhlman, N. E. Solov'ev, G. P. Tsiskarishvili and G. Tsagareishvili, *Boron-rich Solids*, AIP Conf. Proc., **231** (1991) 350.
13. M. Terauchi, R. Kuzuo, F. Satoh, M. Tanaka, K. Tsuno and J. Ohyama, Microsc. Microanal. Microstruct. **2**, 351 (1991).
14. M. Tanaka, M. Terauchi, R. Kuzuo, K. Tsuno, J. Ohyama and Y. Harada, *Proc. 50th Annual Meeting of Electron Microscopy Society of America*, 940 (1992).
15. R. Kuzuo, M. Terauchi, M. Tanaka, Y. Saito, and H. Shinohara, Jpn. J. Appl. Phys., **30** (1991) L1817.
16. R. Kuzuo, M. Terauchi, M. Tanaka, Y. Saito, and H. Shinohara, Trans. Mat. Res. Soc. Jpn., 14B (1994) 1119.
17. R. Kuzuo, M. Terauchi, M. Tanaka, Y. Saito, and H. Shinohara, Phys. Rev. B, **49** (1994) 5054.
18. R. Kuzuo, M. Terauchi, M. Tanaka, Y. Saito, and Y. Achiba, Phys. Rev. B, **51** (1995) 11018.
19. R. F. Egerton, *Electron Energy Loss Spectroscopy in the Electron Microscope*, (Plenum Press, New York, 1986).
20. H. Raether, *Excitation of Plasmons and Interband Transitions by Electrons*, Springer Tract in Modern Physics Vol. 88 (Springer 1980).
21. S. Saito and A. Oshiyama, Phys. Rev. Lett., **66** (1991) 2637.
22. R. Kuzuo, M. Terauchi and M. Tanaka, Jpn. J. Appl. Phys., **31** (1992) L1484.
23. R. Kuzuo, M. Terauchi, M. Tanaka and Y. Saito, Jpn. J. Appl. Phys., **33** (1993) L1316.
24. O. Stéphan, P. M. Ajayan, C. Colliex, F. C. Lackmann and É. Sandré, Phys. Rev. B, **53** (1996) 13824.
25. M. Terauchi, Y. Kawamata, M. Tanaka, M. Takeda and K. Kimura, J. Solid State Chem., in the press.
26. R. Franz and H. Werheit, *Boron-rich Solids*, AIP Conf. Proc. **231**, (1991) 29.
27. C. Feldman, F. Ordway, W. Zimmerman III and K. Moorjani, *Boron* vol. 2, Prenum Press New York, (1965) 235.
28. D. W. Bullett, J. Phys. C **15**, (1982) 415.
29. S. Lee, D. M. Bylander and L. Kleinman, Phys. Rev. B **42**, (1990) 1316.
30. D. Li, Y. N. Xu and W. Y. Ching, Phys. Rev. B **45**, (1992) 5896.

31. M. Fujimori and K. Kimura, J. Solid State Chem., in the press.
32. S. Gunji, Doctor thesis, Science University of Tokyo, (1995) 66.
33. S. Gunji and H. Kamimura, Jpn. J. Appl. Phys. Series **10**, (1994) 35.